Stress triggering of the 2022 Lushan−Maerkang earthquake sequence by historical events and its implication for fault stress evolution in eastern Tibet

Dawei Tang[1], Weipeng Ge[1,2]* and Xiyu Cao[1]

[1]Lanzhou Institute of Seismology, China Earthquake Administration, Lanzhou, China, [2]Gansu Lanzhou National Geophysical Observation and Research Station, Lanzhou, China

It remains unknown how stress triggering causes earthquakes in the eastern Tibetan Plateau following the Wenchuan Earthquake in 2008. The M_S 6.1 Lushan earthquake on 1 June 2022 in a seismic gap between the 2008 M_W 7.9 Wenchuan earthquake and the 2013 M_W 6.6 Lushan earthquake provided an opportunity to detect stress evolution and seismic activity on the fault in this study. We calculated the Coulomb stress change of the June 2022 Lushan−Maerkang earthquake sequence using a Burgers viscoelastic model and, herein, discuss how the sequence have been triggered by historical earthquakes since 1900 in the eastern Tibetan Plateau. Our results suggest the following trends: 1) the 1955 M 7.6 Kangding and 2008 M_W 7.9 Wenchuan earthquakes contributed most significant loading effects on the 2022 M_S 6.1 Lushan earthquake; however, the 2013 M_W 6.6 Lushan earthquake had an unloading effect on the 2022 Lushan earthquake. 2) The 2021 M_W 7.3 Maduo earthquake contributed a loading effect on the 2022 Lushan earthquake, and the 2022 Lushan earthquake may have triggered the subsequent Maerkang earthquake swarm on 10 June 2022. 3) Viscoelastic relaxation of the lower crust and upper mantle contributed significantly to fault stress level, while a fault in a late-phase earthquake cycle may have ruptured *via* slight stress perturbation near a cross-border conversion between positive and negative stress from a far-field earthquake. We also provide a seismic potential assessment along the faults in the eastern Tibet. Notably, the M_W 6.8 Luding earthquake that ruptured the southern segment of the Xianshuihe Fault on 5 September 2022 supports the conclusions of this study.

1 Introduction

An M_S 6.1 earthquake occurred on 1 June 2022, in Lushan County, China. The earthquake hypocenter corresponds to an epicenter of 30.37°N, 102.94°E and a depth of 17 km, according to the China Earthquake Network Center (CENC). Other institutions provided similar, but varying, results (Table 1); for example, the United States Geological Survey (USGS) indicated an epicenter of 30.395°N, 102.958°E, with a moment magnitude of M_W 5.8 and a source depth of 12.0 km, and the Global Centroid Moment Tensor (GCMT)

TABLE 1 Focal mechanisms of the 2022 M$_S$ 6.1 Lushan earthquake given by various research institutions.

Number	Strike (°)/dip (°)/rake (°)		Data source
	NPI	NPII	
1	224/53/105	20/40/71	USGS
2	217/45/103	19/46/78	GCMT
3	211/31/93	28/58/88	GFZ
4	230/62/103	24/31/67	IG
5	220/40/98	29/50/83	IG

IG: Institute of Geophysics, China Earthquake Administration.
GFZ: Helmholtz-Centre Potsdam–German Research Centre for Geosciences.

provided an epicenter of 30.35°N, 103.08°E, with a moment magnitude of M$_W$ 5.8 and a source depth of 21.6 km.

The Lushan M$_S$ 6.1 earthquake in 2022 occurred along the southern segment of the Longmenshan Fault between the Songpan–Ganzi Terrane and the Sichuan Basin (Figure 1)

(Royden et al., 1997; Royden et al., 2008; Zhang et al., 2003; Zhang, 2013; Hubbard and Shaw, 2009; Burchfiel et al., 1995; Clark et al., 2005; Medvedev and Beaumont, 2006; Rui and Stamps, 2016; Densmore et al., 2007; Hu et al., 2012; Luo and Liu, 2018; Chen et al., 2000; Deng et al., 2003). Before the 2008 M$_W$ 7.9 Wenchuan earthquake, the Longmenshan fault zone was in a moderately inactive state due to a slow slip rate (Wang et al., 2010; Burchfiel et al., 2008; Gan et al., 2007; Ma et al., 2005; Wang et al., 2008). However, postseismic deformation after the Wenchuan earthquake became relatively complicated (Huang et al., 2014; Diao et al., 2019; Wang et al., 2021). The 2013 M$_W$ 6.6 Lushan earthquake occurred in the southwest section of the rupture (Jiang et al., 2014). Moreover, the 2022 M$_S$ 6.1 Lushan earthquake occurred in the seismic gap between the 2013 M$_W$ 6.6 Lushan earthquake and the 2008 M$_W$ 7.9 Wenchuan earthquake (Chen et al., 2013; Gao et al., 2014). Therefore, the successive occurrence of these three earthquakes has attracted interest in the scientific community.

Previous studies have indicated that the 2013 Lushan earthquake was located in an area where the Coulomb stress change increased due to the 2008 Wenchuan earthquake and was triggered by that
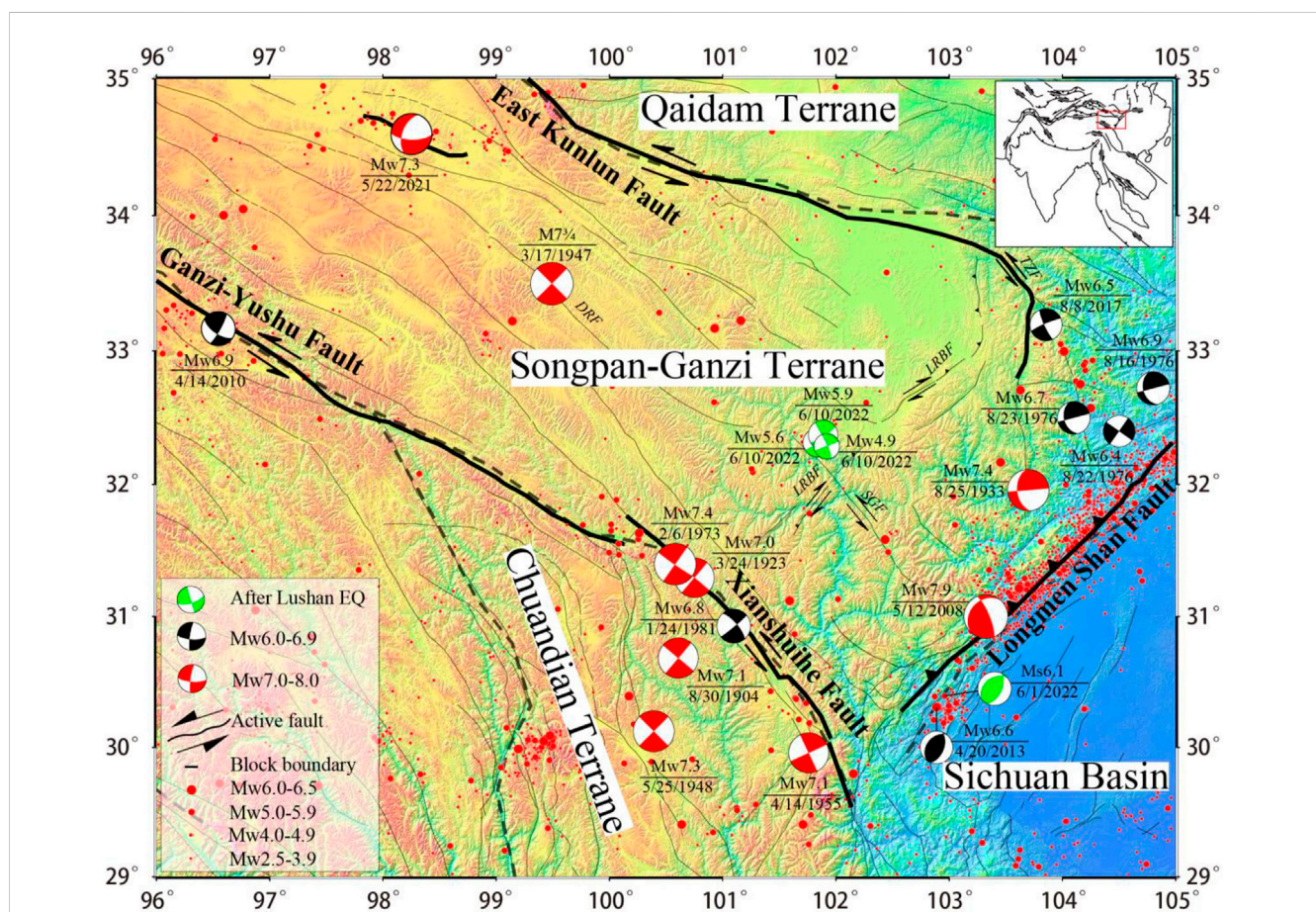
FIGURE 1
Tectonic map of the eastern Tibetan Plateau, southern Qaidam Terrane, Songpan–Ganzi Terrane, northern Chuandian Terrane, and western Sichuan Basin, showing the topography, active faults, and earthquake epicenters. Lower hemisphere diagrams of focal spheres show fault plane solutions from the USGS catalog from January 1904 to July 2022. The green beach balls indicate the 2022 M$_S$ 6.1 Lushan earthquake and the 2022 Maerkang earthquake swarm; the black beach balls indicate the M$_W$ 6.0–6.9 earthquakes; and the nine red beach balls indicate the 1904 M$_W$ 7.1 Daofu earthquake, the 1923 M$_W$ 7.0 Luhuo earthquake, the 1933 M$_W$ 7.4 Diexi earthquake, the 1947 M 7.75 Dari earthquake, the 1948 M$_W$ 7.3 Litang earthquake, the 1955 M$_W$ 7.1 Kangding earthquake, the 1973 M$_W$ 7.4 Luhuo earthquake, the 2008 M$_W$ 7.9 Wenchuan earthquake, and the 2021 M$_W$ 7.3 Maduo earthquake, respectively. The inset shows the tectonic setting of the Indo-Asian collision zone.

TABLE 2 Earthquake rupture parameters.

Historical earthquake	M_w	Strike (°)	Dip (°)	Rake (°)	Length (km)	Width (km)	Average slip (m)	Fault starting coordinates Lat (°N) Lon (°E)	Coseismic ΔCFS (Pa) on 2022 Lushan earthquake	Postseismic ΔCFS (Pa) on 2022 Lushan earthquake	Data source
1904-8-30 Daofu M7.0	7.1	130	90	0	55	18	1.86	31.73 100.82	-2.05×10^2	-9.25×10^2	1, 2
1923-3-24 Luohuo M7.3	7.0	130	90	0	60	14	1.6	31.343 100.659	-6.99×10^2	-3.14×10^3	1, 2
1933-8-25 Diexi M7.5	7.4	175	45	0	90	20	1.98	31.9 103.4	-2.18×10^3	1.77×10^3	3
1947-3-17 Dari M7.75	7.7	135	90	0	252	19	3.1	33.92 98.99	1.88×10^2	2.74×10^3	1, 4
1948-5-25 Litang M7½	7.0	315	90	0	41	20	1.8	29.55 100.52	-1.4×10^2	3.51×10^1	1, 5
1955-4-14 Kangding M7.6	7.1	155	90	0	120	18	2.6781	30.03 101.84	2.21×10^3	7.04×10^3	1, 2
1973-2-06 Luhuo M7.9	7.4	128	87	0	104	17	2.7	31.73 100.19	-1.13×10^3	-2.93×10^3	1, 6
1976-8-16 Songpan M7.2	6.7	165	40	0	30	12	1.3	32.75 104.9	-3.5	-1.2×10^2	3
1976-8-22 Songpan M6.7	6.4	215	90	0	12	8	1.6	32.4 104.5	0.22	5.93	3
1976-8-23 Songpan M7.2	6.7	165	40	0	22	11	1.3	32.5 104.1	-1.95×10^1	-6.1×10^1	3
1981-1-24 Daofu M6.9	6.8	319	73	−4	44	20	0.8	30.7 101.2	-8.22×10^2	-2.77×10^3	1, 7
2008-5-12 Wenchuan M8.0	7.9	229	—	—	315	40	—	32.5224 105.426	2.36×10^4	3.45×10^4	8
2010-4-14 Yushu M7.1	6.9	119	83	11	80	20	0.669	33.209 96.486	-6.28	-4.42×10^1	1, 9
2013-4-20 Lushan M7.0	6.6	214	38	—	66.5	42	—	30.4374 103.289	-4×10^4	-4.53×10^3	10
2017-8-8 Jiuzhaigou $M_W6.5$	6.5	155	81	350	40	30	0.18	33.56 103.71	4.57	-3.8	1, 3
2021-5-22 Maduo $M_W7.3$	7.3	106	76	—	182	31.5	—	34.8176 97.3406	9.26×10^1	1.3×10^2	8
2022-6-1 Lushan M6.1	6.0	230	37	109	11.5	7.1	0.51	30.395 102.958	—	—	8

TABLE 2 (*Continued*) Earthquake rupture parameters.

Historical earthquake	M_W	Strike (°)	Dip (°)	Rake (°)	Length (km)	Width (km)	Average slip (m)	Fault starting coordinates Lat (°N) Lon (°E)	Coseismic ΔCFS (Pa) on 2022 Lushan earthquake	Postseismic ΔCFS (Pa) on 2022 Lushan earthquake	Data source
2022-6-10 Maerkang M5.8	5.6	325.66	76.26	−4.5	8	5.7	0.23	32.315 101.836	—	—	8
2022-6-10 Maerkang M6.0	5.9	323	68	−16	12.2	6.8	0.36	32.373 101.872	—	—	8
2022-6-10 Maerkang M5.2	4.9	338.42	83.53	−0.04	3	3.6	0.087	32.287 101.918	—	—	8

1: Wells and Coppersmith (1994); 2: Wen et al. (2008); 3: Wang and Xu (2017); 4: Molnar and Deng (1984); 5: Zhou et al. (2015); 6: Tang et al. (1976); 7: Cheng (1983); 8: USGS (erthquake.usgs.gov); 9: Wen et al. (2013); 10: Li et al. (2017).

earthquake (Toda et al., 2008; Lei et al., 2013; Jia K et al., 2014; Liu et al., 2014; Wang et al., 2014; Xie et al., 2014; Zhu and Miao, 2015; Zhu, 2016; Lin et al., 2019). If a triggering correlation exists, it is unclear why the 2022 Lushan earthquake occurred 9 years later. The potential seismogenic trend of faults around the Longmenshan fault system is also in question. The Lushan earthquake and Maerkang earthquake swarm that occurred in June 2022 provided a significant opportunity to study the correlation of earthquake triggering. Therefore, we studied the stress triggering of the 2022 Lushan earthquake and the three subsequent Maerkang earthquakes from the events shown in Table 2. Herein, we discuss the subsequent seismic trend of surrounding faults and the triggering pattern of the Lushan–Maerkang earthquake sequence *via* historical earthquakes.

2 Data and method

2.1 Stratified viscoelastic model

We used a stratified viscoelastic model to simulate the Songpan–Ganzi Terrane, where earthquakes mainly occur along the Longmenshan Fault. The wave velocity and density structure of the crust and upper mantle were taken from Jia S et al. (2014) and Xu et al. (2010). We assumed that the thickness of the elastic layer of the crust was 30 km, and that the viscoelastic material was below that depth. The viscosity coefficient mainly refers to the rheological structural parameters of the lithosphere in eastern Tibet obtained by Wang et al. (2021) based on deformation simulation after the 2008 M_W 7.9 Wenchuan earthquake, as shown in Table 3.

The Maxwell body and Kelvin body in rheological structures have defects in fitting short-term and long-term deformation, respectively. Therefore, we chose the Burgers body, which is suitable for simulating transient elastic response, short-term exponential decay response, and long-term linear increase response (Pollitz and Wicks, 2001; Pollitz and Sacks, 2002; Shao et al., 2007). The constitutive relation (Malkin and Isayev, 2022) is as follows:

$$\sigma + \left(\frac{\eta_2}{k_1} + \frac{\eta_1}{k_1} + \frac{\eta_2}{k_2}\right)\dot{\sigma} + \frac{\eta_1\eta_2}{k_1 k_2}\ddot{\sigma} = \eta_2\dot{\varepsilon} + \frac{\eta_1\eta_2}{k_1}\ddot{\varepsilon} \qquad (1)$$

where σ is the stress, ε is the strain, and k_1 and k_2 are the stiffness coefficients of the Kelvin model and Maxwell model, respectively. η_1 and η_2 are the Kelvin model viscosity (short-term viscosity) and Maxwell model viscosity (long-term viscosity), respectively. k_2, the effective stiffness coefficient, is obtained from the S-wave velocity and density of the medium, and the incomplete relaxation stiffness coefficient is $k_1 = \alpha k_2 / (1 - \alpha)$, in which α is set to 0.67, according to Ryder et al. (2011). Unless otherwise specified, the Coulomb stress change mentioned in this paper is the sum of coseismic and postseismic viscoelastic relaxation.

2.2 Method

The formula for calculating the Coulomb failure stress change on the fault plane is as follows (King et al., 1994; Harris, 1998):

$$\Delta \text{CFS} = \Delta\tau + \mu'\Delta\sigma_n \qquad (2)$$

TABLE 3 Parameters of the crust and upper mantle.

Number	Layer name	Thickness (km) (from Wang et al., 2021)	$V_p/(km/s)$	$V_S(km/s)$	$\rho/(kg \cdot cm^{-3})$	$\eta_1/\left(P_a \cdot s\right)$	$\eta_2/\left(P_a \cdot s\right)$
1	Upper crust	0–10	6.05	3.2	2,500	∞	∞
2	Middle crust	10–30	6.2	3.5	2,850	∞	∞
3	Lower crust	30–55	6.55	3.6	2,950	5×10^{17}	5×10^{18}
4	Upper mantle	55–500	7.9	3.9	3,280	5×10^{18}	1×10^{19}

where $\Delta\tau$ is the shear stress change on the fault plane (taking the fault sliding direction as positive), $\Delta\sigma_n$ is the normal stress change on the fault plane (the tension is positive), and μ' is the effective friction coefficient of the fault. The effective friction coefficient is 0.4 (King et al., 1994). We used the PSGRN/PSCMP program for this work (Wang et al., 2006).

2.3 Coseismic slip model

The stress field induced by an earthquake can be calculated using fault dislocation theory and the source fault slip model. The Coulomb stress change on the receiving fault plane can be obtained using Formula (1). In our study, we used two methods to obtain the slip model of the source fault: one method used the existing accurate slip distribution model of an earthquake, such as that of the 2021 M_W 7.3 Maduo earthquake released by the USGS; in the second method, the empirical formula of the relationship between the fault length and magnitude was obtained using statistics (Wells and Coppersmith, 1994), the scalar seismic distance formula, and the moment magnitude definition formula (Knopoff, 1958; Hanks and Kanamori, 1979):

The thrust earthquake equations are as follows (coefficients are the average values):

$$logRLD = 0.58Mw - 2.42 \ (4.8 < Mw < 7.6) \quad (3)$$
$$logRW = 0.41Mw - 1.61 \ (4.8 < Mw < 7.6) \quad (4)$$

The strike–slip earthquake equations are as follows (coefficients are the average values):

$$logRLD = 0.62Mw - 2.57 \ (4.8 < Mw < 8) \quad (5)$$
$$logRW = 0.27Mw - 0.76 \ (4.8 < Mw < 7.6) \quad (6)$$
$$M_0 = \mu \cdot RLD \cdot RW \cdot \bar{D} \quad (7)$$
$$M_W = \frac{2}{3}(\log M_0 - 9.1) \quad (8)$$

where RLD is the length of the fault along the strike direction, RW is the width of the fault along the dip direction, M_W is the magnitude of the moment, M_0 is the scalar seismic moment, μ is the shear modulus of the medium, and $\bar{D}$ is the average dislocation of the fault. According to the existing seismic fault parameters, the length, width, and average dislocation of the fault can be calculated using Formulas 3ormulas –Formulas 8. See Table 2 for the specific seismic fault rupture parameters.

Afterslip on historical earthquake faults can affect some simulation results (Nur and Mavko, 1974). However, we did not consider the afterslip effect in the calculation; compared with the main earthquake, the contribution of afterslip is concentrated in the near field, and the stress change it causes is much smaller than the effect of the coseismic slip model (Shen et al., 2009; 2011; Wang et al., 2011).

3 Results

3.1 Triggering effect on Coulomb stress change in the 2022 Lushan earthquake

We calculated the coseismic and postseismic viscoelastic Coulomb stress change effects of historical earthquakes on the 2022 Lushan earthquake using the seismic rupture parameters, as shown in Table 2. We show the Coulomb stress change at a depth of 12 km, which is also the result of waveform fitting, and from the USGS. The focal mechanism parameter of the receiving fault is the result from the USGS in Table 1.

The postseismic shear stress change ($\Delta\tau$) at the hypocenter of the 2022 Lushan earthquake (30.395°N, 102.958°E) was positive (consistent with the direction of fault slip), which contributed to fault rupture (Figure 2A). The normal stress change ($\Delta\sigma_n$) at the hypocenter was in the negative shadow zone (Figure 2B), indicating that the 2008 Wenchuan earthquake caused a significant extrusion change in the fault normal direction, which was not prone to fault instability. The Coulomb stress change (ΔCFS) at the hypocenter was in the positive shadow zone (Figure 2C), so the 2008 Wenchuan earthquake had a very obvious loading effect on the 2022 Lushan earthquake. According to Table 2, the coseismic ΔCFS of the 2008 Wenchuan earthquake on the 2022 Lushan earthquake was 2.36×10^4 Pa, and the ΔCFS at the time of the 2022 Lushan earthquake occurrence was 3.45×10^4 Pa, indicating that the loading effect of the 2008 Wenchuan earthquake on the 2022 Lushan earthquake increased with ongoing loading of the viscoelastic lower crust and upper mantle.

The hypocenter of the 2022 Lushan earthquake was near the cross-border conversion between positive and negative $\Delta\tau$, but had positive values (Figure 2G). The hypocenter of the 2022 Lushan earthquake was near the $\Delta\sigma_n$ cross-border conversion between positive and negative, but had negative values (Figure 2H). The hypocenter of the 2022 Lushan earthquake was in the negative shadow zone of ΔCFS (Figure 2I), so the 2013 Lushan earthquake had an unloading effect on the 2022 Lushan earthquake. The coseismic ΔCFS of the 2013 Lushan on the 2022 Lushan
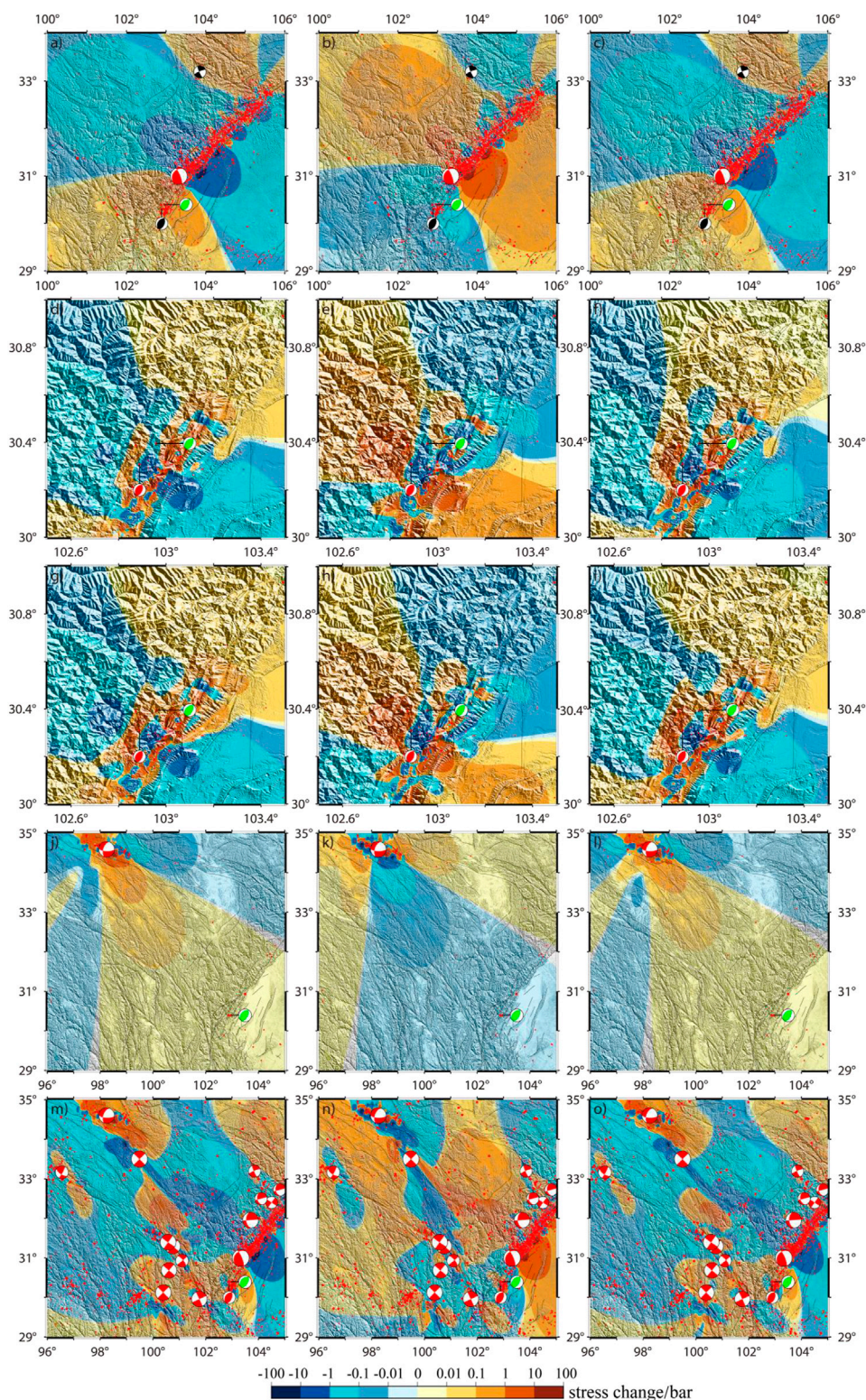
FIGURE 2
Contour map of Coulomb stress change in the 2022 Lushan earthquake. The red beach balls are the source events, the green beach balls are the receiving events, and the black beach balls are events between the source and receiving events. **(A–C)** Effects of postseismic shear stress change, normal stress change, and Coulomb stress change of the 2008 Wenchuan earthquake on the 2022 Lushan earthquake, respectively. **(D–F)** Same display (coseismic) as for effects of the 2013 Lushan earthquake on the 2022 Lushan earthquake. **(G–I)** Same display (postseismic) as for effects of the 2013 Lushan earthquake on the 2022 Lushan earthquake. **(J–L)** Same display (postseismic) as for effects of the 2021 Maduo earthquake on the 2022 Lushan earthquake. **(M–O)** Same display (postseismic) as for effects of historical earthquakes on the 2022 Lushan earthquake.
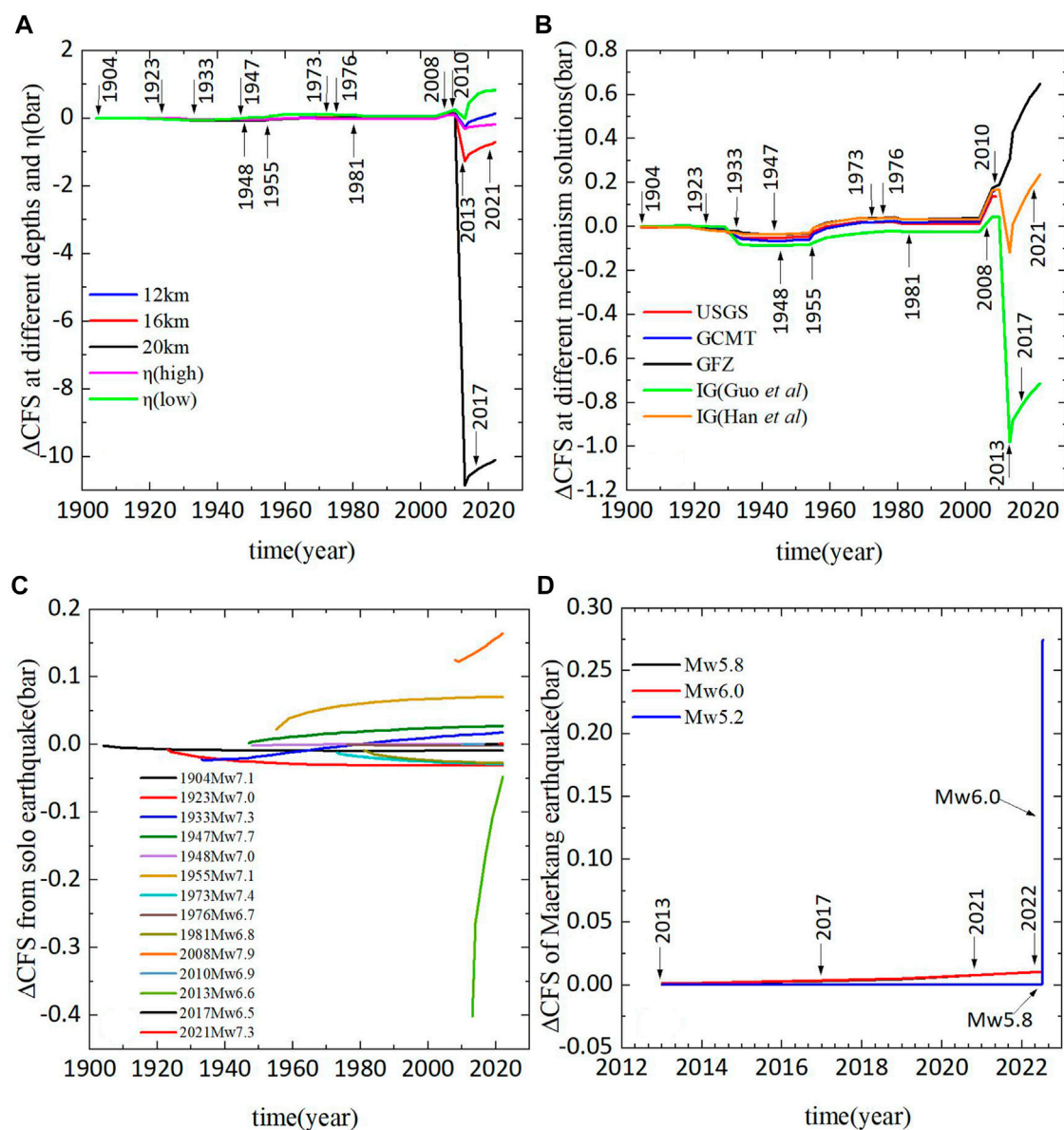
FIGURE 3
Trend of the viscoelastic ΔCFS over time. **(A)** ΔCFS trend at the epicenter of the 2022 Lushan earthquake for different depths and viscosities. **(B)** ΔCFS trend at the epicenter of the 2022 Lushan earthquake with different focal mechanism solutions. **(C)** ΔCFS trend at the epicenter of the 2022 Lushan earthquake from each historical earthquake. **(D)** ΔCFS trend at the epicenters of the three 2022 Maerkang earthquakes.

earthquake was −4×10⁴ Pa, and this negative value then decreased to −4.53×10³ Pa. These data are consistent with the coseismic and postseismic stress change evolution of the 2013 Lushan earthquake (Figures 2D–I). The viscoelastic lower crust and upper mantle contributed to the occurrence of the 2022 Lushan earthquake.

The postseismic Δτ, Δσ$_n$, and ΔCFS contour maps show that the 2021 Maduo earthquake had loading effects on the 2022 Lushan earthquake that were similar to those of the Wenchuan earthquake, as shown in Figures 2J–L. The coseismic ΔCFS of the Maduo earthquake on the 2022 Lushan earthquake was 9.26×10¹ Pa, and the postseismic ΔCFS increased to 1.3×10² Pa at the time of the 2022 Lushan earthquake.

Under the combined effects of historical earthquakes, the Δτ at the hypocenter of the 2022 Lushan earthquake was positive, and the Δσ$_n$ was negative. Due to their combined effects, all of which were near the cross-border conversion between positive and negative stress change of the three, ΔCFS was positive (Figures 2M–O). The overall ΔCFS value was high, and the accumulated seismic moment was at a high level. Therefore, under the influence of the 2021 Maduo earthquake, the 2022 Lushan earthquake occurred along the southwest section of the Longmenshan Fault.

Figure 3C shows the evolution of ΔCFS of historical earthquakes on the 2022 Lushan earthquake alone. As shown by the solid blue
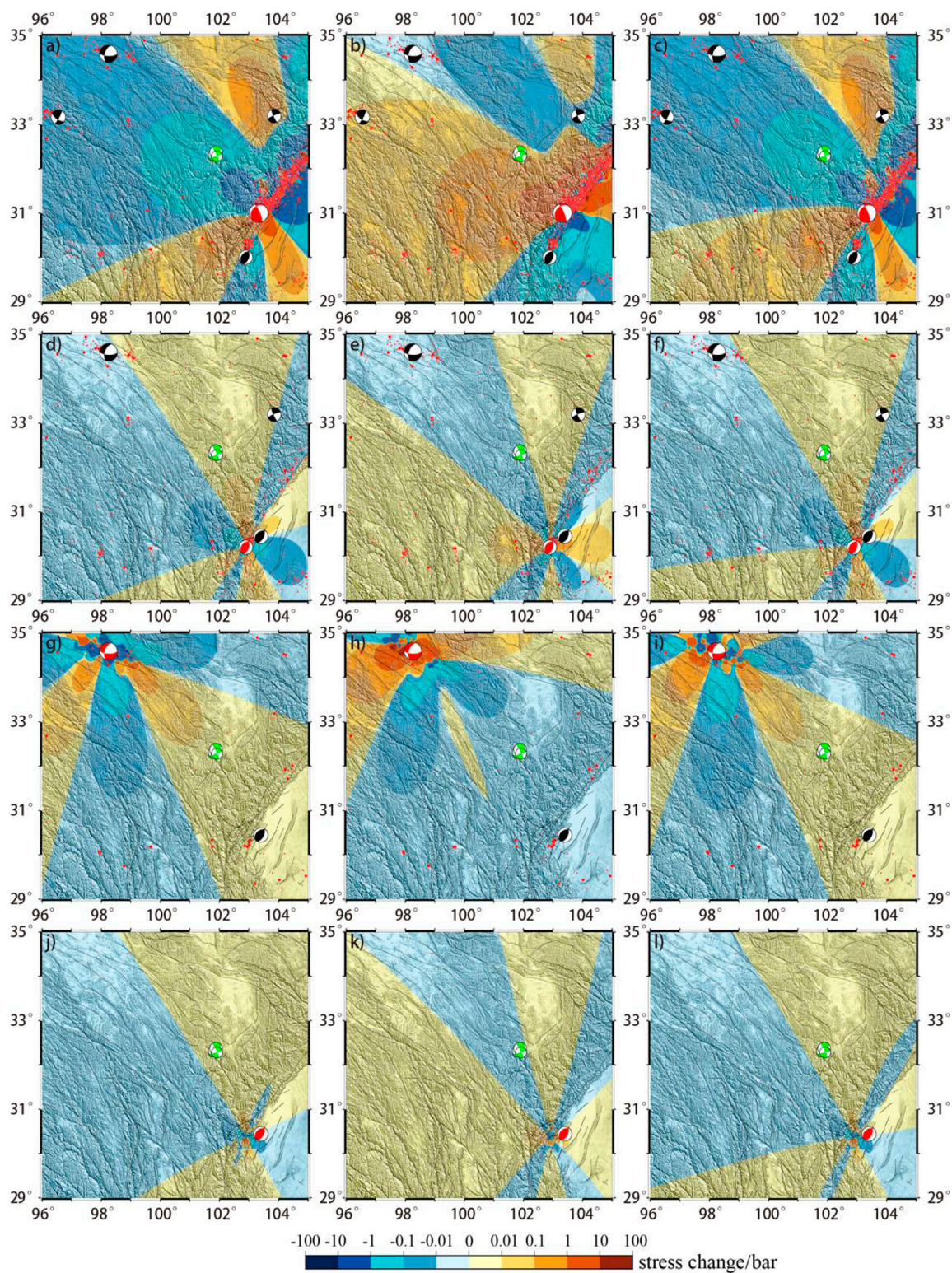
FIGURE 4
Contour map of Coulomb stress change in the 2022 Maerkang earthquakes. The red beach balls are source events, the green beach balls are receiving events, and the black beach balls are events between the source and receiving events. **(A–C)** Effects of the postseismic shear stress change, normal stress change, and Coulomb stress change of the 2008 Wenchuan earthquake on the 2022 Maerkang earthquakes. **(D–F)** Same display as for effects of the 2013 Lushan earthquake on the 2022 Maerkang earthquakes. **(G–I)**: Same display as for effects of the 2021 Maduo earthquake on the 2022 Maerkang earthquakes. **(J–L)** Same display as for effects of the 2022 Lushan earthquake on the 2022 Maerkang earthquakes.
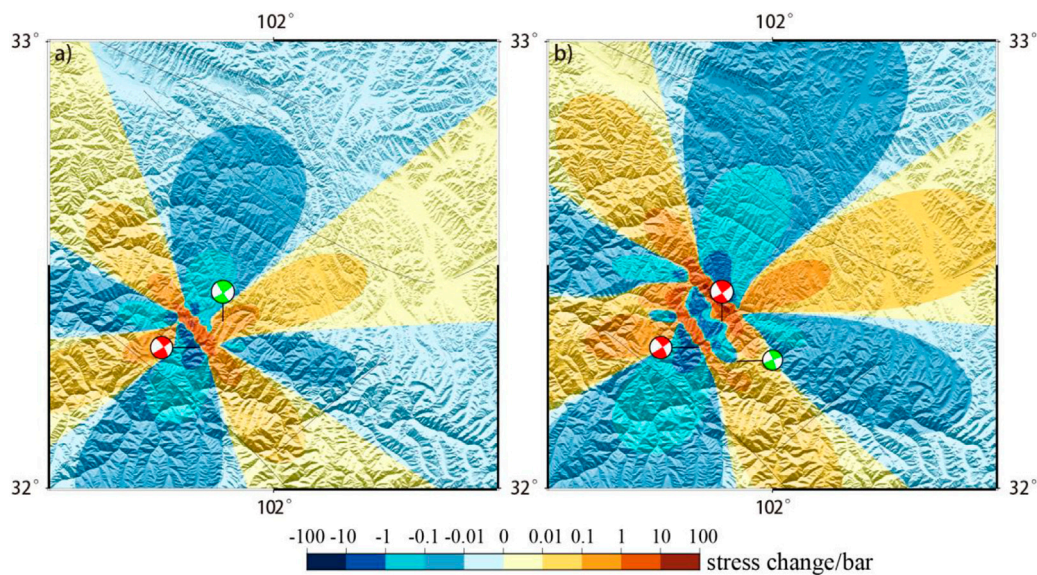
FIGURE 5
Contour map of the Coulomb stress change in the three successive Maerkang earthquakes in 2022. **(A)** Coseismic Coulomb stress change in the M_W 5.6 Maerkang earthquake resulting from the M_W 5.9 Maerkang earthquake. **(B)** Coseismic Coulomb stress change of the M_W 4.9 Maerkang earthquake resulting from the M_W 5.6 and M_W 5.9 Maerkang earthquakes.

line (12 km) in (A) and (C), the ΔCFS remained at a small positive value due to the great distance from the previous historical earthquakes. However, after the 2008 Wenchuan earthquake, the ΔCFS rapidly increased to exceed the threshold value of 0.1 bar (King et al., 1994; Harris, 1998); the coseismic effect of the 2013 Lushan earthquake then caused it to decrease to a negative value. Under the continuous viscoelastic relaxation of the lower crust and upper mantle, the ΔCFS went from negative to positive, resulting in the M_S 6.1 earthquake that occurred on 1 June 2022. This pattern may also explain why the M_S 6.1 earthquake gap did not rupture when the 2013 Lushan earthquake occurred. In summary, Table 2 and Figure 3 show that the loading effect of the 2008 Wenchuan earthquake on the 2022 Lushan earthquake was dominant in these historical earthquakes, while the unloading effect was dominant in the 2013 Lushan earthquake.

3.2 Triggering effect on Coulomb stress change in the Maerkang earthquakes

After the Lushan M_S 6.1 earthquake on 1 June 2022, the M_W 5.6 (MEK1), M_W 5.9 (MEK2), and M_W 4.9 (MEK3) earthquakes occurred within a few hours on 10 June 2022 in Maerkang County. The three successive earthquakes were very close in time and space. We studied the triggering effect on Coulomb stress change using the earthquake rupture parameters in Table 2.

We considered a stress change at a depth of 10 km, consistent with the hypocenter depth given by the USGS. The focal mechanism solutions of the three earthquakes in Maerkang were equivalent and similar, and these solutions can be regarded as a single event (MEK1) under the action of historical earthquakes.

The Δτ and ΔCFS at the MEK1 hypocenter was negative, which was not conducive to fault slip (Figures 4A, C). The Δσ_n was positive, indicating that the normal stress change of the Maerkang earthquakes caused by the Wenchuan earthquake changed significantly (Figure 4B), which contributed to the instability of the fault.

The hypocenter of MEK1 was near the cross-border conversion between positive and negative Δτ, and its value was positive (Figure 4D). The hypocenter of MEK1 was also near the cross-border conversion between positive and negative Δσ_n, and its value was negative (Figure 4E). The hypocenter of MEK1 was in the ΔCFS positive shadow area (Figure 4F), so the 2013 Lushan earthquake may have triggered the 2022 Maerkang earthquake. Remarkably, the focal mechanism solutions of the 2021 Maduo earthquake and the 2017 Jiuzhaigou earthquake, similar to that of the Maerkang earthquake, were also located near the positive and negative cross-border conversion of shear stress change and normal stress change caused by the 2013 Lushan earthquake. This finding indicates that the 2013 Lushan earthquake might also have triggered the 2017 Jiuzhaigou earthquake and the 2021 Maduo earthquake.

The triggering effect of the 2022 Lushan earthquake was similar as shown in Figures 4J–L, the Δτ and Δσ_n at the hypocenter of the 2022 Maerkang earthquake included one positive and one negative value, but the ΔCFS was entirely in the positive shadow area. Therefore, the 2021 Maduo earthquake also had a certain loading effect on the 2022 Maerkang earthquakes to that of the 2013 Lushan earthquake Figures 4G-I.

According to Figure 5, the MEK2 was located in the ΔCFS positive shadow area caused by the MEK1, which triggered the MEK2, and the MEK3 was located near the cross-border conversion between positive and negative ΔCFS caused by the MEK1 and
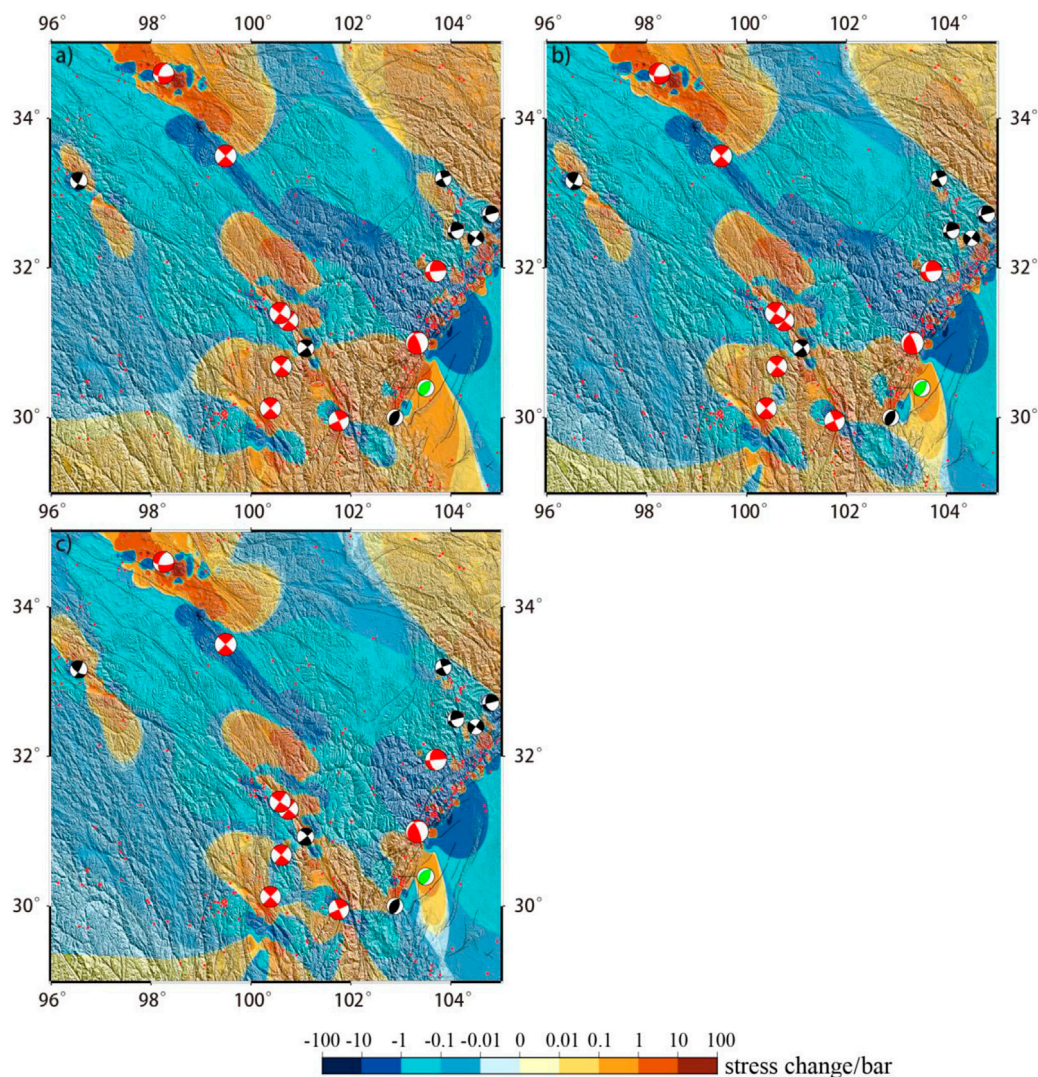
FIGURE 6
Impact of the viscosity coefficient, with low viscosity, normal viscosity, and high viscosity, on the Coulomb stress change contour map of the 2022 Lushan earthquake due to historical earthquakes. **(A)** Contour map of Coulomb stress change at low viscosity. **(B)** Contour map of Coulomb stress change at normal viscosity. **(C)** Contour map of Coulomb stress change at high viscosity.

MEK2, indicating that the MEK1 and MEK2 may have jointly triggered the MEK3.

The hypocenter of the Lushan-Maerkang earthquake sequence seems to have been near the cross-border conversion between positive and negative stress change. It appears that the stress change at the hypocenter experienced a transform from negative to positive when the hypocenter finally became a starting point of rupture and the earthquake occurred. This phenomenon has been confirmed by Freed (2005), whose work showed that the hypocenter of the 1999 Hector Mine earthquake was very close to the border between positive and negative Coulomb stress change caused by the 1992 Landers earthquake. In addition, Xie et al. (2022) found that the hypocenter of the 2011 M_S 9.0 Tokyo earthquake was located near the border between positive and negative normal stress change. We assumed that the positive and negative changes in stress were more likely to cause the rock at the hypocenter to plastically fail and thereby cause an earthquake.

4 Discussion

4.1 Effect of model viscosity parameters on the results

The viscosity of the lower crust and upper mantle in the Tibetan Plateau and its surrounding areas has been studied over the past two decades. Clark and Royden (2000) used the topographic gradient method to estimate the viscosity beneath the lower crust around the Tibetan Plateau and obtained approximate results of $10^{16} \sim 10^{21}$ Pa s. Shao et al. (2011) considered the viscoelastic relaxation effect of the
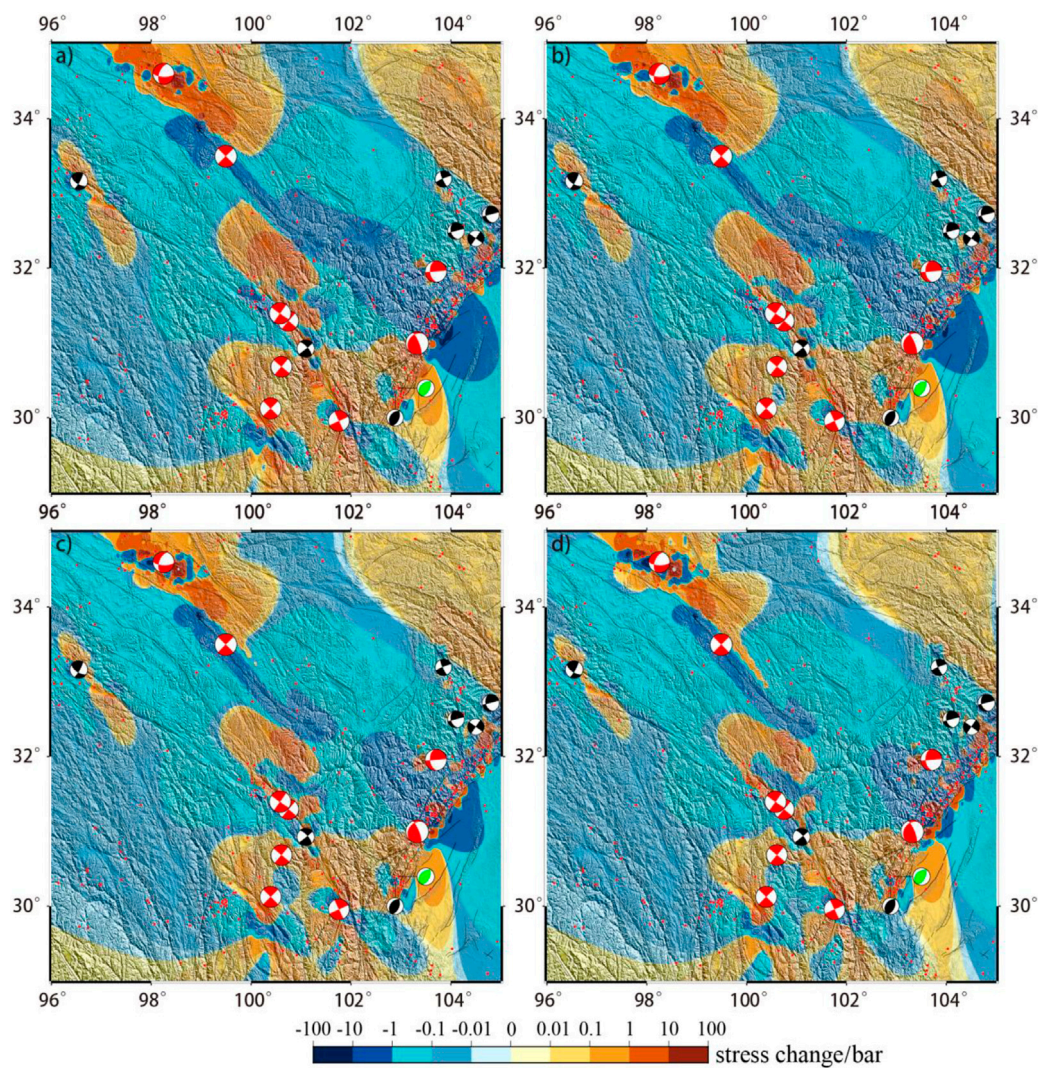
FIGURE 7
Impact of effective friction coefficients of 0.2, 0.4, 0.6, and 0.8 on the Coulomb stress change contour map of the Lushan earthquake in 2022 by historical earthquakes. **(A–D)** Contour maps of Coulomb stress change with effective friction coefficients of 0.2, 0.4, 0.6, and 0.8, respectively.

lower crust and upper mantle after the 2008 Wenchuan earthquake. They found that the best long-term viscosity coefficient of the lower crust and upper mantle in the Songpan–Ganzi Terrane was 5×10^{17} Pa s. Huang et al. (2014) used GPS and InSAR data to constrain the 1.5-year postseismic deformation of the 2008 Wenchuan earthquake and found that the long-term viscosity coefficient of the upper mantle of the Songpan–Ganzi Terrane was 1×10^{18} Pa s. Zhao et al. (2021) determined that the transient viscosity and steady viscosity of the lower crust and upper mantle in Tibet were 5×10^{18} Pa s and 4×10^{19} Pa s, respectively, through crustal deformation simulation after the 2001 Kekexili earthquake. Wei et al. (2020) estimated the viscosity range beneath the lower crust in the West Qinling–Songpan Terrane and its surrounding areas by a geomorphological analysis method and channel flow model, and the result was $10^{18} \sim 10^{20}$ Pa s. Wang et al. (2021) strictly constrained the long-term viscosity of the lower

crust and upper mantle in the Songpan–Ganzi Terrane to $(4.3–5.7) \times 10^{18}$ Pa s and $(1–1.6) \times 10^{18}$ Pa s according to the GPS data after the Wenchuan earthquake. Currently, the viscosity value of the lower crust and upper mantle in the eastern Tibetan Plateau remains controversial, as the viscosity at different time scales changes, but it is concentrated in the range of $10^{18} \sim 10^{20}$ Pa s. Therefore, testing of different viscosity coefficients is necessary.

We used the latest results from Wang et al. (2021) and tested the influence of two groups of viscosities (one order of magnitude lower and one order of magnitude higher) on the Coulomb stress change calculation results, as shown in Figures 6A–C. The ΔCFS evolution at the hypocenter of the 2022 Lushan earthquake using the three groups of viscosities is shown in Figure 3A. Variation in viscosity can induce different Coulomb stress changes, but it has little influence on the distribution range and evolution trend of ΔCFS. Therefore, the viscosity conditions considered in our study were appropriate.
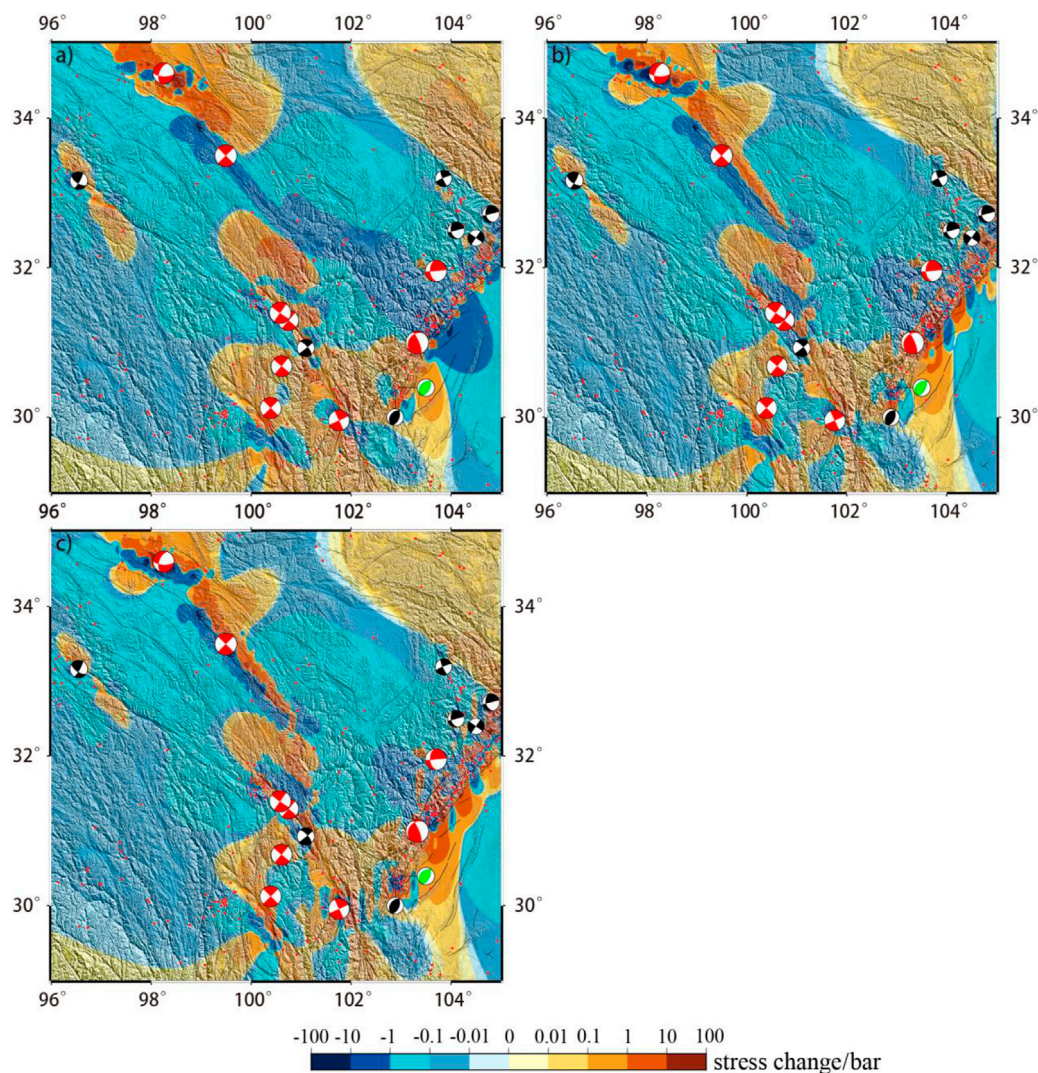
FIGURE 8
Impacts of historical earthquakes, at depths of 12 km, 16 km, and 20 km, on the Coulomb stress change contour map of the Lushan earthquake in 2022. **(A)** Contour map of Coulomb stress change at a depth of 12 km. **(B)** Contour map of Coulomb stress change at a depth of 16 km. **(C)** Contour map of Coulomb stress change at a depth of 20 km.

4.2 Effect of the effective friction coefficient

The effective friction coefficient in Formula (2), involving the pore fluid and medium of the fault plane, is an uncertain parameter in Coulomb stress change calculations (King et al., 1994; Harris, 1998; Tang et al., 2023), and it is important to discuss the influence of its sensitivity on the results. King et al. (1994) proposed that the effective friction coefficients are generally 0.2–0.8. Shen (2003) showed that the effective friction coefficient of most faults can change only the relative magnitude of ΔCFS, but cannot affect the polarity of ΔCFS.

To ensure the reliability of our results, we calculated the influence of the four groups of effective friction coefficients, i.e., 0.2, 0.4, 0.6, and 0.8, on the Coulomb stress change. As the effective friction coefficient increased from 0.2 to 0.8, the

distribution range of Coulomb stress change in the 2022 Lushan earthquake area showed little variation (Figure 7). The ΔCFS at the hypocenter of the 2022 Lushan earthquake was still near the border between positive and negative stress change, but the value was positive. This result shows that the ΔCFS changes with the effective friction coefficient. However, the change in the effective friction coefficient in our study does not alter our conclusion.

4.3 Effect of depth on the results

Previous studies focused on the triggering effect of Coulomb stress change between earthquakes with stress fields at the depth of the hypocenter (Freed and Lin, 2001; Cheng, 2018; Li et al., 2022; Stein, 1999). However, hypocenter depth is difficult to estimate. The USGS
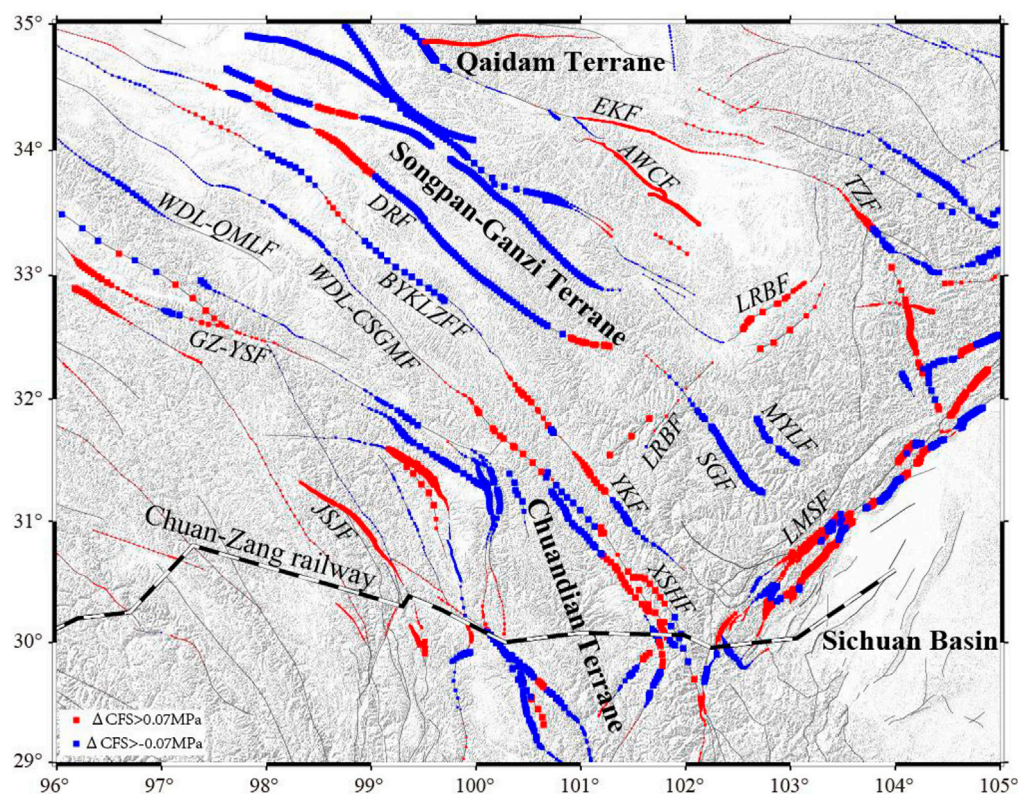
FIGURE 9
Contour map of the Coulomb stress change along faults around the Songpan−Ganzi Terrane effected by historical earthquakes. Abbreviations of major faults: East Kunlun Fault (EKF), Tazan Fault (TZF), Wancang Fault (AWCF), Dari Fault (DRF), Longba Fault (LRBF), Wudaoliang−Qumalai Fault (WDL-QMLF), Wudaoliang−Changshagongma Fault (WDL-CSGMF), Bayankalazhufeng Fault (BYKLZFF), Ganzi−Yushu Fault (GZ-YSF), Miyaluo Fault (MYLF), Songpan−Ganzi Fault (SGF), Jinshajiang Fault (JSJF), Yuke Fault (YKF), Xianshuihe Fault (XSHF), Longmenshan Fault (LMSF), Sichuan−Tibet railway (Chuan-Zang railway).

suggested two hypocenter depths of 12 km and 19.5 km for the 2022 M_S 6.1 Lushan earthquake, and the GFZ and the CENC suggested hypocenter depths of 10 km and 17 km. respectively. For strike−slip faults, the change in the Coulomb stress field with depth is small (Wan et al., 2007), but the Longmenshan Fault is under oblique-strike motion. Thus, the contribution of the Coulomb stress change on fault planes with different depths is discussed in further detail here.

As shown in Figure 8, the ΔCFS at the epicenter of the 2022 Lushan earthquake was calculated for depths of 12 km, 16 km, and 20 km. The ΔCFS distribution range of the Longmenshan area varies significantly with depth. The 2022 Lushan earthquake occurred near the cross-border conversion between positive and negative stress change, but the ΔCFS value changed from positive to negative as the depth increased. Combined with Figure 3A, the ΔCFS evolution curves of the 2022 Lushan earthquake epicenter at different depths were consistent and coincided before 2013. However, the 2013 Lushan earthquake caused great differences at different depths. On the fault of the 2022 Lushan earthquake, the historical earthquakes had a strong unloading effect at a depth of 20 km, but a slight unloading effect at depths of 16 km and 12 km. Therefore, ΔCFS may vary at different depths on the fault plane. Thus, the influence of different hypocenter depths requires further study.

4.4 Effect of the focal mechanism solution of the receiving fault on the results

We evaluated focal mechanism solutions from the USGS. As shown in Figure 3B, the fluctuations in the curves of different focal mechanism solutions were similar. However, the effects of the 2013 Lushan earthquake on the 2022 Lushan earthquake using the GFZ solution were quite different from those of the other four groups. The large uncertainties in the strike and dip angle in the GFZ inversion results may be the source of the discrepancy. Therefore, the collection of focal mechanism solutions considered in our study greatly influenced the calculated results. We suggest that, when a similar calculation of fault stress change is carried out to study the interaction mechanism between strong earthquakes, focal mechanism solutions as similar as possible to actual earthquakes should be considered.

4.5 Influence of the Lushan−Maerkang earthquake sequence and historical earthquakes on the faults around the Songpan−Ganzi Terrane

We calculated the Coulomb stress change along the faults around the Songpan−Ganzi Terrane after the Lushan−Maerkang

earthquake sequence in 2022. The fault slip data were from previous publications (Deng, 2007; Xu et al., 2016, https://www.activefault-datacenter.cn/map).

Figure 9 shows the Coulomb stress change induced by historical earthquakes on the faults in the Songpan–Ganzi Terrane at a depth of 10 km. The eastern section of the East Kunlun fault zone and the central section of the Longriba fault zone are in a continuous zone of high Coulomb stress change, which is consistent with the results of Cheng (1983) and Wang and Xu (2017). The western section of the Songgang Fault lies along an area in which ΔCFS changes sign, which corresponds to the occurrence of the Maerkang earthquake swarm in 2022. Additionally, the southern section of the Xianshuihe Fault has a higher ΔCFS value, similar to the ΔCFS distribution along the Xianshuihe Fault in Liu e al. (2014). The M_S 6.8 Luding earthquake that occurred on 5 September 2022 also confirmed our prediction.

Furthermore, the middle section of the Yuke Fault, the southern section of the Xianshuihe Fault, the eastern section of the Dari Fault, the Bayankala Fault, the Wudaoliang–Changshagongma Fault, and the Chuan–Zang railway are near areas in which the ΔCFS changes sign, therefore potential earthquake risk may be high.

5 Conclusion

We constructed a stratified viscoelastic model to simulate postseismic stress on the 2022 Lushan–Maerkang earthquake sequence from historical strong earthquake data in eastern Tibet. We further assessed the seismic potential of faults in eastern Tibet. Our conclusions are as follows.

(1) The 1955 M 7.6 Kangding and 2008 M_W 7.9 Wenchuan earthquakes are the most significant loading events on the 2022 M_S 6.1 Lushan earthquake. But, the 2013 M_W 6.6 Lushan earthquake is the most significant unloading event. This is a potential explanation for the occurrence of the 2022 Lushan earthquake 9 years later. Effects of viscoelastic relaxation of the lower crust and upper mantle play a significant role in fault activity.

(2) The M_W 5.6, M_W 5.9, and M_W 4.9 Maerkang earthquakes, which occurred after the 2022 Lushan earthquake, could have been due to both the 2013 and 2022 Lushan earthquakes. The 2021 Maduo earthquake had a loading effect on the 2022 Lushan earthquake, and the 2022 Lushan earthquake might have triggered the Maerkang earthquakes. Furthermore, the M_W 5.6 Maerkang earthquake may have triggered the M_W 5.9 Maerkang earthquake, and the M_W 5.6 and M_W 5.9 Maerkang earthquakes may have jointly triggered the M_W 4.9 Maerkang earthquake.

(3) The tectonic stress of the Songpan–Ganzi Terrane has accumulated to a high level. The hypocenters of the 2022 Lushan–Maerkang earthquake sequence all occurred near the cross-border conversion between positive and negative stress change. Rupture of a fault in a late phase of the seismic cycle near the cross-border conversion between positive and negative stress change may have been induced by a slight stress disturbance from a far-field earthquake. Therefore, study of the the middle section of the Yuke Fault, the southern section of the Xianshuihe Fault (which has been confirmed by the 5 September 2022, M_W 6.8 Luding earthquake), the eastern section of the Dari Fault, the Bayankala Fault, and the Wudaoliang–Changshagongma Fault should be emphasized in future research, as they all correspond to areas of cross-border conversion.

Data availability statement

The original contributions presented in the study are included in the article/Supplementary Material, and further inquiries can be directed to the corresponding author.

Author contributions

DT and WG conceived the study and wrote the manuscript. XC helped archive fault trace data. All authors discussed, commented on, and edited the manuscript.

Funding

Acknowledgments

Conflict of interest

The authors declare that the research was conducted in the absence of any commercial or financial relationships that could be construed as a potential conflict of interest.

Publisher's note

All claims expressed in this article are solely those of the authors and do not necessarily represent those of their affiliated organizations, or those of the publisher, the editors, and the reviewers. Any product that may be evaluated in this article, or claim that may be made by its manufacturer, is not guaranteed or endorsed by the publisher.

References

Burchfiel, B. C., Royden, L. H., Hilst, R. D. V. D., Hager, B. H., Chen, Z., King, R. W., et al. (2008). A geological and geophysical context for the wenchuan earthquake of 12 may 2008, sichuan, people's Republic of China. *Geol. Soc. Am.* 18, 4. doi:10.1002/2013GC005067

Burchfiel, B. C., Zhiliang, C., Yupinc, L., and Royden, L. H. (1995). Tectonics of the Longmen Shan and adjacent regions, central China. *Int. Geol. Rev.* 37 (8), 661–735. doi:10.1080/00206819509465424

Chen, Y. T., Yang, Z. X., Zhang, Y., and Liu, C. (2013). From 2008 Wenchuan earthquake to 2013 Lushan earthquake (in Chinese). *Sci. Sin. Terrae* 43, 1064–1072. doi:10.1360/zd-2013-43-6-1064

Chen, Z., Burchfiel, B. C., Liu, Y., King, R. W., Royden, L. H., Tang, W., et al. (2000). Global Positioning System measurements from eastern Tibet and their implications for India/Eurasia intercontinental deformation. *J. Geophys. Res.* 105, 16215–16227. B7, 16, 215–16. doi:10.1029/2000JB900092

Cheng, Erlin. (1983). Source parameters of Daofu earthquke (Ms=6.9) sichuan province on january 24, 1981[J]. *Chin. J. Geophys. (in Chinese)* 26 (02), 140–148.

Cheng, J., Yao, S., Liu, J., Yao, Q., Gong, H., and Long, H. (2018). Visoelastic Coulomb stress of historical earthquakes on the 2017 Jiuzhaigou earthquake and the subsequent influence on the seismic hazards of adjacent faults. *Chinese Journal of Geophysics (in Chinese)* 61 (5), 2133–2151. doi:10.6038/cjg2018L0609

Clark, M. K., and Royden, L. H. (2000). Topographic ooze: Building the eastern margin of Tibet by lower crustal flow. *Geology* 28 (8), 703–706. doi:10.1130/0091-7613(2000)28<703:TOBTEM>2.0.CO;2

Clark, M. K., Bush, J. W., and Royden, L. H. (2005). Dynamic topography produced by lower crustal flow against rheological strength heterogeneities bordering the Tibetan Plateau. *Geophysical Journal International* 162 (2), 575–590. doi:10.1111/j.1365-246X.2005.02580.x

Deng, Qidong. (2007). *China active tectonic map(1:40000000)*. Beijing: Seismological Press. ISBN:9787502830519.

Deng, Q., Zhang, P., Ran, Y., Yang, X., Min, W., and Chu, Q. (2003). Basic characteristics of active tectonics of China. Science in China Series D. *Earth Sciences* 46 (4), 356–372. doi:10.3321/j.issn:1006-9267.2002.12.007

Densmore, A. L., Ellis, M. A., Li, Y., Zhou, R., Hancock, G. S., and Richardson, N. (2007). Active tectonics of the Beichuan and Pengguan faults at the eastern margin of the Tibetan Plateau. *Tectonics* 26, TC4005. doi:10.1029/2006TC001987

Diao, F., Xiong, X., Wang, R., Walter, T. R., Wang, Y., and Wang, K. (2019). Slip rate variation along the Kunlun fault (Tibet): Results from new GPS observations and a viscoelastic earthquke-cycle deformation model. *Geophysical Research Letters* 46 (5), 2524–2533. doi:10.1029/2019GL081940

Freed, A. M., and Lin, J. (2001). Delayed triggering of the 1999 Hector Mine earthquake by viscoelastic stress transfer. *Nature* 411 (6834), 180–183. doi:10.1038/35075548

Freed, A. M. (2005). Earthquake triggering by static, dynamic, and postseismic stress transfer. *Annual Review of Earth and Planetary Sciences* 33 (1), 335–367. doi:10.1146/annurev.earth.33.092203.122505

Gan, W., Zhang, P., Shen, Z. K., Niu, Z., ang, M. W., an, Y. W., et al. (2007). Present-day crustal motion within the Tibetan Plateau inferred from GPS measurements. *Geophys. Res. Solid Earth Planets* 112, B08416. doi:10.1029/2005JB004120

Gao, Y., Wang, Q., Zhao, B., and Shi, Y. (2014). A rupture blank zone in middle south part of Longmenshan Faults: Effect after Lushan M s7.0 earthquake of 20 April 2013 in Sichuan, China. *China. Science China Earth Sciences* 57 (9), 2036–2044. doi:10.1007/s11430-014-4827-2

Hanks, T. C., and Kanamori, H. (1979). A moment magnitude scale. *Journal of Geophysical Research Solid Earth* 84 (5), 2348–2350. doi:10.1029/JB084iB05p02348)

Harris, R. A. (1998). Introduction to special section: Stress triggers, stress shadows, and implications for seismic hazard. *Journal of Geophysical Research Solid Earth* 103 (10), 24347–24358. doi:10.1029/98JB01576

Hu, Caibo, Cai, Y., and Wang, Z. (2012). Effects of large historical earthquakes, viscous relaxation, and tectonic loading on the 2008 Wenchuan earthquake. *Journal of Geophysical Research* 117, 6. doi:10.1029/2011jb009046

Huang, M. H., Bürgmann, R., and Freed, A. M. (2014). Probing the lithospheric rheology across the eastern margin of the Tibetan Plateau. *Earth and Planetary Science Letters* 396, 88–96. doi:10.1016/j.epsl.2014.04.003

Hubbard, J., and Shaw, J. H. (2009). Uplift of the longmen Shan and Tibetan plateau, and the 2008 wenchuan (M= 7.9) earthquake. *Nature* 458 (7235), 194–197. doi:10.1038/nature07837

Jia, K., Zhou, S., Zhuang, J., and Jiang, C. (2014). Possibility of the independence between the 2013 lushan earthquake and the 2008 wenchuan earthquake on longmen Shan fault, sichuan, China. *Seismol. Res. Lett.* 85, 60–67. doi:10.1785/0220130115

Jia S S., Liu, B., Xu, Z., Liu, Z., Feng, S., Zhang, J., et al. (2014). The crustal structures of the central Longmenshan along and its margins as related to the seismotectonics of the 2008 Wenchuan Earthquake. *Science China Earth Sciences* 57 (4), 777–790. doi:10.1007/s11430-013-4744-9

Jiang, Z., Wang, M., Wang, Y., Wu, Y., Che, S., Shen, Z. K., et al. (2014). GPS constrained coseismic source and slip distribution of the 2013 Mw6. 6 Lushan, China, earthquake and its tectonic implications. *Geophysical Research Letters* 41 (2), 407–413. doi:10.1002/2013GL058812

King, G. C. P., Stein, R. S., and Lin, J. (1994). Static stress changes and the triggering of earthquakes[J]. *Bulletin of the Seismological Society of America* 84 (3), 935–953. doi:10.1016/0148-9062(95)94484-2

Knopoff, L. (1958). Energy release in earthquakes. *Geophysical Journal International*, 1(1): 44–52. doi:10.1111/j.1365-246x.1958.tb00033.x

Lei, X. L., Ma, S. L., Su, J. R., and Wang, X. L. (2013). Inelastic triggering of the 2013 M W 6.6 Lushan earthquake by the 2008 M W 7.9 Wenchuan earthquake. *Seismology and Geology* 35 (2), 411–422. doi:10.3969/j.issn.0253-4967.2013.02.019

Li, J., Liu, C., Zheng, Y., and Xiong, X. (2017). Rupture process of the Ms 7.0 Lushan earthquake determined by joint inversion of local static GPS records, strong motion data, and teleseismograms. *Journal of Earth Science* 28 (2), 404–410. doi:10.1007/s12583-017-0757-1

Li, Y., Shao, Z., Hu, X., Shi, F., Liu, H., and Chen, L. W. (2022). Stress and strain characteristics in the seismic region of the M6.1 Nakchu earthquake on March 19, 2021 and their geodynamic implications. *Chinese Journal of Geophysics (in Chinese)* 65 (2), 673–685. doi:10.6038/cjg2022P026912

Lin, X., Chu, R., and Zeng, X. (2019). Rupture processes and Coulomb stress changes of the 2017 Mw 6.5 Jiuzhaigou and 2013 Mw 6.6 Lushan earthquakes. *Earth, Planets and Space* 71 (1), 81–15. doi:10.1186/s40623-019-1061-3

Liu, M., Luo, G., and Wang, H. (2014). The 2013 Lushan earthquake in China tests hazard assessments. *Seismological Research Letters* 85 (1), 40–43. doi:10.1785/0220130117

Luo, G., and Liu, M. (2018). Stressing rates and seismicity on the major faults in eastern Tibetan Plateau. *Journal of Geophysical Research Solid Earth* 123 (12), 10. doi:10.1029/2018JB015532

Ma, B., Su, G., Hou, Z., and Su, S. B. (2005). Late quaternary slip rate in the central part of the Longmenshan fault zone from terrace deformation along the Minjiang River. *Seismol. Geol.* 27, 234–242. doi:10.3969/j.issn.0253-4967.2005.02.006

Malkin, A. Y., and Isayev, A. I. (2022). *Rheology: Concepts, methods, and applications*. Netherlands: Elsevier. doi:10.1007/978-1-4612-1428-1_7

Medvedev, S., and Beaumont, C. (2006). Growth of continental plateaus by channel injection: Models designed to address constraints and thermomechanical consistency. *Geological Society, London, Special Publications* 268 (1), 147–164. doi:10.1144/GSL.SP.2006.268.01.06

Molnar, P., and Denq, Q. (1984). Faulting associated with large earthquakes and the average rate of deformation in central and eastern Asia. *John Wiley and Sons, Ltd* 89 (7), 6203–6227. doi:10.1029/JB089iB07p06203)

Nur, A., and Mavko, G. (1974). Postseismic viscoelastic rebound. *Science* 183 (4121), 204–206. doi:10.1126/science.183.4121.204

Pollitz, F. F., and Wicks, C. (2001). Mantle flow beneath a continental strike-slip fault: Postseismic deformation after the 1999 hector mine earthquake. *science* 293 (5536), 1814–1818. doi:10.1126/science.1061361

Pollitz, F. F., and Sacks, I. S. (2002). Stress triggering of the 1999 Hector Mine earthquake by transient deformation following the 1992 Landers earthquake. *Bulletin of the Seismological Society of America* 92 (4), 1487–1496. doi:10.1785/0120000918

Royden, L. H., Burchfiel, B. C., King, R. W., Wang, E., Chen, Z., Shen, F., et al. (1997). Surface deformation and lower crustal flow in eastern Tibet. *science* 276 (5313), 788–790. doi:10.1126/science.276.5313.788

Royden, L. H., Burchfiel, B. C., and van der Hilst, R. D. (2008). The geological evolution of the Tibetan Plateau. *science* 321 (5892), 1054–1058. doi:10.1126/science.1155371

Rui, X., and Stamps, D. S. (2016). Present-day kinematics of the eastern Tibetan Plateau and Sichuan Basin: Implications for lower crustal rheology. *Journal of Geophysical Research Solid Earth* 121 (5), 3846–3866. doi:10.1002/2016JB012839

Ryder, I., Bürgmann, R., and Pollitz, F. (2011). Lower crustal relaxation beneath the Tibetan Plateau and Qaidam basin following the 2001 kokoxili earthquake. *Geophysical Journal International* 187 (2), 613–630. doi:10.1111/j.1365-246X.2011.05179.x

Shao, Z., Fu, R., Xue, T., and Huang, J. (2007). Simulating postseismic viscoelastic deformation based on Burgers model. *Journal of Geodesy and Geodynamics* (05), 31–37. doi:10.3969/j.issn.1671-5942.2007.05.007

Shao, Z., Wang, R., Wu, Y., and Zhang, L. (2011). Rapid afterslip and short-term viscoelastic relaxation following the 2008 M_W7. 9 Wenchuan earthquake. *Earthquake Science* 24 (2), 163–175. doi:10.1007/s11589-010-0781-z

Shen, Z. (2003). Viscoelastic triggering among large earthquakes along the East Kunlun fault system[J]. *Chinese Journal of Geophysics (in Chinese)* 46 (6), 786–795. doi:10.3321/j.issn:0001-5733.2003.06.010

Shen, Z. K., Sun, J., Zhang, P., Wan, Y., Wang, M., Bürgmann, R., et al. (2009). Slip maxima at fault junctions and rupturing of barriers during the 2008 Wenchuan earthquake. *Nature geoscience* 2 (10), 718–724. doi:10.1038/NGEO636

Shen, Z., Wang, F., Wang, M., Wan, Y., Zhang, P., Sun, J., et al. (2011). Postseismic deformation of the 2008 Mw 7.9 Wenchuan earthquake and its tectonic implications. *AGU Fall Meeting Abstracts* 2011, T31E–T07.

Stein, R. S. (1999). The role of stress transfer in earthquake occurrence. *Nature* 402 (6762), 605–609. doi:10.1038/45144

Tang, D., Ge, W., Yuan, D., Zheng, W., and Hu, C. (2023). Triggering effect of historical earthquakes in the northern Tibetan Plateau on the Coulomb stress of the 2022 Menyuan MS6.9 earthquake and subsequent earthquakes. *Chinese Journal of Geophysics*. (in Chinese). doi:10.6038/cjg2023Q0400

Tang, R., Wen, D., Deng, T., and Huang, S. (1976). A preliminary study on the characteristics of the ground fractures during the Luhuo M=7.9 earthquake, 1973 and the origin of the earthquake[J]. *Chinese Journal of Geophysics (in Chinese)* 19 (01), 18–27.

Toda, S., Lin, J., Meghraoui, M., and Stein, R. S. (2008). 12 May 2008 M= 7.9 Wenchuan, China, earthquake calculated to increase failure stress and seismicity rate on three major fault systems. *Geophysical Research Letters* 35 (17), L17305. doi:10.1029/2008gl034903

Wan, Y., Shen, Z., Zeng, Y., and Sheng, S. (2007). Evolution of cumulative failure stress in Northern Qinghai-Xizang (Tibetan) plateau and its effect on large earthquake occurrence. *Acta Seismol Sinica* (02), 115–129. doi:10.3321/j.issn:0253-3782.2007.02.001

Wang, H., Liu, M., Shen, X., and Liu, J. (2010). Balance of seismic moment in the songpan-ganze region, eastern Tibet: Implications for the 2008 great wenchuan earthquake. *Tectonophysics* 491 (1-4), 154–164. doi:10.1016/j.tecto.2009.09.022

Wang, J-J., and Xu, C-J. (2017). Coseismic Coulomb stress changes associated with the 2017 MW6.5 Jiuzhaigou earthquake (China) and its impacts on surrounding major faults. *Chinese Journal of Geophysics (in Chinese)* 60 (11), 4398–4420. doi:10.6038/cjg20171127

Wang, M., Shen, Z. K., Wang, Y. Z., Bürgmann, R., Wang, F., Zhang, P. Z., et al. (2021). Postseismic deformation of the 2008 Wenchuan earthquake illuminates lithospheric rheological structure and dynamics of eastern Tibet. *Journal of Geophysical Research Solid Earth* 126 (9), e2021JB022399. doi:10.1029/2021JB022399

Wang, Q., Qiao, X., Lan, Q., Freymueller, J, Shaomin, Y., Caijun, X., et al. (2011). Rupture of deep faults in the 2008 Wenchuan earthquake and uplift of the Longmen Shan. *Nature Geoscience* 4 (9), 634–640. doi:10.1038/ngeo1210

Wang, R., Lorenzo-Martin, F., and Roth, F. (2006). PSGRN/PSCMP—A new code for calculating co-and post-seismic deformation, geoid and gravity changes based on the viscoelastic-gravitational dislocation theory. *Computers and Geosciences* 32 (4), 527–541. doi:10.1016/j.cageo.2005.08.006

Wang, Y., Wang, E., Shen, Z., Wang, M., Gan, W., Qiao, X., et al. (2008). GPS-constrained inversion of present-day slip rates along major faults of the Sichuan-Yunnan region, China. *Science in China Series D Earth Sciences* 51 (9), 1267–1283. doi:10.1007/s11430-008-0106-4

Wang, Y., Wang, F., Wang, M., Shen, Z. K., and Wan, Y. (2014). Coulomb stress change and evolution induced by the 2008 Wenchuan earthquake and its delayed triggering of the 2013 Mw 6.6 Lushan earthquake. *Seismological Research Letters* 85 (1), 52–59. doi:10.1785/0220130111

Wei, C., Ge, W., and Zhang, B. (2020). Estimating the lower crustal viscosity of the Western Qilian-Songpan Tectonic Node and its adjacent areas by using landform morphology. *Seismology and Geology* 42 (1), 163. doi:10.3969/j.issn.0253-4967.2020.01.011

Wells, D. L., and Coppersmith, K. J. (1994). New empirical relationships among magnitude, rupture length, rupture width, rupture area, and surface displacement. *Bulletin of the seismological Society of America* 84 (4), 974–1002. doi:10.1785/BSSA0840040974

Wen, X. Z., Ma, S. L., Xu, X. W., and He, Y. N. (2008). Historical pattern and behavior of earthquake ruptures along the eastern boundary of the Sichuan-Yunnan faulted-block, southwestern China. *Physics of the Earth and Planetary Interiors* 168 (1-2), 16–36. doi:10.1016/j.pepi.2008.04.013

Wen, Y., Xu, C., Liu, Y., Jiang, G., and He, P. (2013). Coseismic slip in the 2010 Yushu earthquake (China), constrained by wide-swath and strip-map InSAR. *Natural Hazards and Earth System Sciences* 13 (1), 35–44. doi:10.5194/nhess-13-35-2013

Wessel, P., and Smith, W. H. F. (1998). New, improved version of generic mapping tools released. Eos. *Transactions American Geophysical Union* 79 (47), 579. doi:10.1029/98eo00426

Xie, Chao-Di, Xing-Lin, L., Wu, X-P., Hu, X-L., Zhao, Xiao-Yan, and Zhu, R-H. (2014). The effect on the nucleation and failure of MS7.0 Lushan earthquake induced by the MS8.0 Wenchuan earthquake. *Chinese Journal of Geophysics (in Chinese)* 57 (6), 1825–1835. doi:10.6038/cjg20140614

Xie, Z., Cai, Y., Yoshioka, S., and Abe, D. (2022). Exploring the location of large earthquakes using fault stress accumulation—a case study upon M W 9.0 tohoku-oki earthquake in Japan. *Chinese Journal of Geophysics* (1), 1–11. doi:10.6038/cjg2022P0727

Xu, X. W., Han, Z. J., Yang, X. P., Zhang, S., Yu, G., Zhou, B., et al. (2016). *Seismotectonic map in China and its adjacent regions*. Beijing: Seismological Press.

Xu, Y., Li, Z., Huang, R., and Xu, Y. (2010). Seismic structure of the Longmen Shan region from S-wave tomography and its relationship with the Wenchuan Ms 8.0 earthquake on 12 May 2008, southwestern China. *Geophysical Research Letters* 37 (2). doi:10.1029/2009GL041835

Zhang, P. Z. (2013). A review on active tectonics and deep crustal processes of the Western Sichuan region, eastern margin of the Tibetan Plateau. *Tectonophysics* 584, 7–22. doi:10.1016/j.tecto.2012.02.021

Zhang, P. Z., Deng, Q. D., Zhang, G. M., Ma, J., Gan, W. J., Min, W., et al. (2003). Strong earthquake activity and active land mass in mainland China. *Scientia Sinica (Terrae)* S 1, 12–20. doi:10.3321/j.issn:1006-9267.2003.z1.002

Zhao, D., Qu, C., Bürgmann, R., Gong, W., and Shan, X. (2021). Relaxation of Tibetan lower crust and afterslip driven by the 2001 Mw7. 8 Kokoxili, China, earthquake constrained by a decade of geodetic measurements. *Journal of Geophysical Research Solid Earth* 126 (4), e2020JB021314. doi:10.1029/2020JB021314

Zhou, C., Wu, Z., Zhang, K., Li, J., Jiang, Y ., Tian, T., et al. (2015). New chronological constraint on the co-seimic surface rupture segments associated with the Litang Fault. *Seismology and Geology* 37 (2), 455. doi:10.3969/j.issn.0253-4967.2015.02.009

Zhu, S. (2016). Is the 2013 Lushan earthquake (Mw= 6.6) a strong aftershock of the 2008Wenchuan, China mainshock (Mw= 7.9)? *Journal of Geodynamics* 99, 16–26. doi:10.1016/j.jog.2016.05.002

Zhu, S., and Miao, M. (2015). How did the 2013 lushan earthquake (Ms= 7.0) trigger its aftershocks? Insights from static Coulomb stress change calculations. *Pure and Applied Geophysics* 172 (10), 2481–2494. doi:10.1007/s00024-015-1064-3